BIOCHEMISTRY
including biophysical chemistry & molecular biology
Article

Biochemistry **2009,** *48,* 6305–6317 6305
DOI: 10.1021/bi900436v

Characterization of the Covalent and Noncovalent Adducts of Agp1 Phytochrome Assembled with Biliverdin and Phycocyanobilin by Circular Dichroism and Flash Photolysis[†]

Berthold Borucki,*[,‡] Sven Seibeck,[‡] Maarten P. Heyn,[‡] and Tilman Lamparter[§,∥]

[‡]*Biophysics Group, Department of Physics, Freie Universität Berlin, Arnimallee 14, 14195 Berlin, Germany, and* [§]*Institute of Plant Physiology, Department of Biology, Freie Universität Berlin, Königin-Luise-Strasse 12, 14195 Berlin, Germany* [∥]*Present address: Institute of Botany, Department of Biology, Universität Karlsruhe, Kaiserstr. 2, 76131 Karlsruhe, Germany.*

Received March 13, 2009; Revised Manuscript Received June 2, 2009

ABSTRACT: The functional role of the covalent attachment of the bilin chromophores biliverdin (BV) and phycocyanobilin (PCB) was investigated for phytochrome Agp1 from *Agrobacterium tumefaciens* using circular dichroism (CD) and transient absorption spectroscopy. Covalent and noncovalent adducts with these chromophores were prepared by using wild-type (WT) Agp1 (covalent BV and noncovalent PCB binding), mutant C20A in which the covalent BV binding site is eliminated, and mutant V249C in which the covalent PCB binding site is introduced. While the CD spectra of the P_r forms of all these photochromic adducts are qualitatively the same, the CD spectrum of the P_{fr} form of the covalent PCB adduct is unique in having a positive rotational strength in the Q-band which we assign to the $Z-E$ isomerization of the C−D methine bridge. In the three other adducts, the Q-band CD in the P_{fr} state is almost zero, suggesting that upon photoconversion a negative contribution from an out-of-plane rotation of the A ring of the chromophore compensates for the positive contribution from ring D. The contribution from ring A is absent or strongly reduced in the shorter π-conjugation system of the covalent PCB adduct. The results from CD spectroscopy are consistent with a uniform geometry of the bilin chromophore in the covalent and noncovalent adducts. Transient absorption spectroscopy showed that the spectral changes and the kinetics of the P_r to P_{fr} photoconversion are not substantially affected by the covalent attachment of BV and PCB. The kinetics in the BV and PCB adducts mainly differ in the formation of P_{fr} that is accelerated by 2 orders of magnitude in the PCB adducts, whereas the sequence of spectral transitions and the associated proton transfer processes are quite similar. We conclude that the P_r to P_{fr} photoconversion in the BV and PCB adducts of Agp1 involves the same relaxation processes and is thus governed by specific protein−cofactor interactions rather than by the chemical structure of the chromophore or the mode of attachment. The strongly reduced photostability of the noncovalent BV adduct suggests that covalent attachment in native Agp1 phytochrome prevents irreversible photobleaching and stabilizes the chromophore. The N-terminal peptide segment including amino acids 2−19 is essential for covalent attachment of the chromophore but dispensable for the spectral and kinetic properties of Agp1.

Phytochromes are biliprotein photoreceptors that were originally discovered in plants where they control many developmental processes such as seed germination, de-etiolation, or the onset of flowering (*1*). Extensive genome sequencing and studies with recombinant proteins have shown that phytochromes and phytochrome-like proteins also exist in many cyanobacteria, proteobacteria, and fungi (*2*). Typical phytochromes have a PAS,[1] GAF, and PHY domain at the N-terminus; the C-terminal part often contains a histidine kinase or, in plant phytochromes, a histidine kinase-like domain (see Figure 1B for the arrangement of the domains). Phytochromes carry a bilin chromophore which is covalently attached to the protein. Depending on the species, three different bilin (open chain tetrapyrrole) chromophores can be used: biliverdin (BV), phytochromobilin (PϕB), or phycocyanobilin (PCB). BV binding phytochromes were found in many bacteria, including cyanobacteria, and in fungi (*3*−*7*).

[†]This work was supported by grants of the Deutsche Forschungsgemeinschaft to B.B. and M.P.H. (BO 1911/1-2) and T.L. (Sfb 498, TP B2).

*To whom correspondence should be addressed. E-mail: borucki@physik.fu-berlin.de. Fax: +49-30-8385 6299. Phone: +49-30-8385 5191.

[1]Abbreviations: BV, biliverdin IXα; PCB, phycocyanobilin; PϕB, phytochromobilin; SVD, singular-value decomposition; PAS, acronym formed from the names of the first three proteins recognized as sharing this sensory domain; GAF, abbreviation derived from cGMP-specific phosphodiesterases, cyanobacterial adenylate cyclases, and transcription activator FhlA; PHY domain, domain specific for phytochromes; CBD, chromophore-binding domain, including PAS and GAF domains; IAA, iodoacetamide; DNTB, 5,5′-dithiobis(2-nitrobenzoic acid); DMSO, dimethyl sulfoxide.

Published on Web 06/04/2009

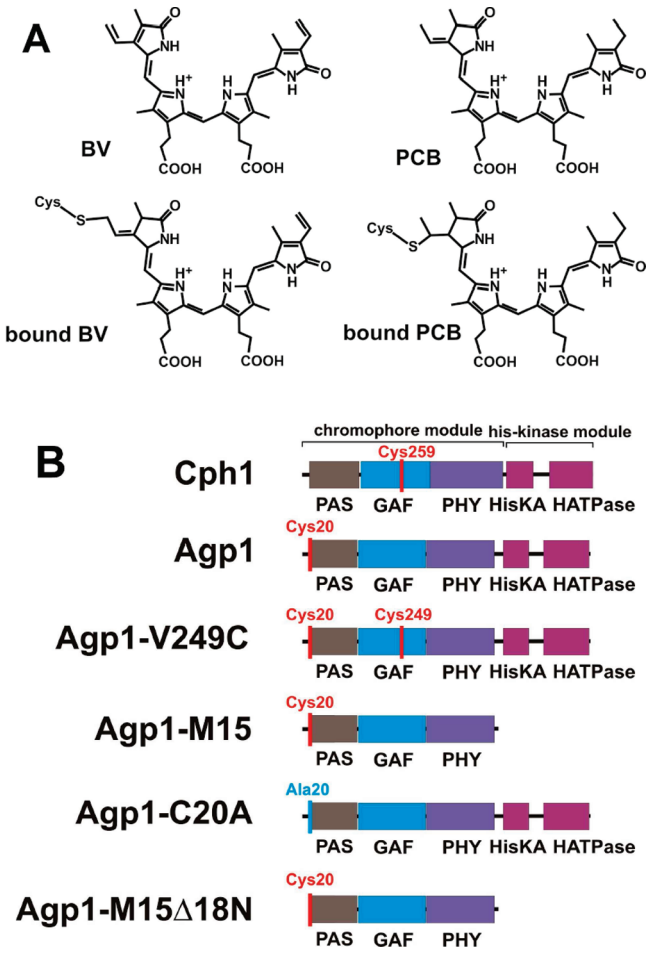

FIGURE 1: (A) Chemical structures of the BV and PCB chromophores covalently and noncovalently attached to the protein. The configuration/conformation is $5Z_{syn},10Z_{syn},15Z_{anti}$ as identified in the recently determined three-dimensional structures of bacteriophytochromes and Cph1. (B) Nomenclature and domain arrangement of Cph1 and the Agp1 variants and fragments used in this study. The positions of the binding sites of the BV and PCB chromophores in Agp1, Cys20 and Cys249, respectively, are indicated. In Cph1, the PCB chromophore binds to Cys259.

The chemical structures of the free and bound forms of BV and PCB are shown in Figure 1A. PCB is used as a chromophore in many cyanobacterial phytochromes and a green alga (*8*, *9*), whereas PϕB is the chromophore of land plants (*10*). During evolution, the replacement of the chromophore was apparently coupled to an exchange of the chromophore binding cysteine (*11*). In BV-binding phytochromes, a cysteine which is located at the N-terminus of the PAS domain is used for covalent attachment (*4*, *12*) (Figure 1B). This cysteine forms a thioether link with the ring A vinyl side chain (*13*). PCB and PϕB binding phytochromes use a cysteine in the GAF domain for chromophore binding (Figure 1B). In these cases, a thioether link is formed with the ethylidene side chain of bilin ring A. However, covalent binding is not a prerequisite for chromophore incorporation. In vitro, three different ways can lead to noncovalent binding of the chromophore (*4*): the chromophore binding Cys is (i) mutated to another amino acid or (ii) blocked by chemicals such as IAA, or (iii) the apoprotein is mixed with a chromophore which has an unsuitable substituent at ring A.

Phytochromes display photochromic behavior involving two almost thermostable states, P_r and P_{fr}, with distinct absorption spectra that can be reversibly interconverted by red and far-red light, respectively. The P_r to P_{fr} photoconversion is associated with a rapid $Z-E$ isomerization (picoseconds) around the $C_{15}=C_{16}$ bond (*14*−*17*) followed by a series of slower (microseconds to milliseconds) conformational transitions in the dark (*18*−*21*). The intermediates in the thermal relaxation cascade are named Lumi-R, Meta-R_A, and Meta-R_C according to low-temperature studies of plant phytochromes (*22*, *23*). There are many cases in which adducts with noncovalently bound chromophores undergo normal P_r to P_{fr} and P_{fr} to P_r photoconversion and dark reversions (*4*, *24*−*27*). For the noncovalent Agp1−PCB adduct, it has been shown that the light modulation of His kinase activity is comparable with that of the covalent BV adduct (*4*, *28*). Thus, intramolecular signal transduction is also not dependent on covalent chromophore attachment. However, all natural phytochromes characterized so far bind the chromophore in a covalent manner, suggesting that there is a strong evolutionary pressure on the covalent binding of the chromophore in phytochromes.

Recently, the three-dimensional structures of the CBDs of phytochromes from *Deinococcus radiodurans* (*29*, *30*) and *Rhodopseudomonas palustris* (*31*) in the P_r state were determined. The BV chromophore is bound via a thioether linkage between the conserved N-terminal cysteine side chain and the $C3^2$ atom of the ring A vinyl group and adopts a $5Z_{syn},10Z_{syn},15Z_{anti}$ configuration/conformation. The geometry of the A−B and C−D methine bridges is in agreement with the results from assembly studies of Agp1 in solution with sterically locked BV derivatives (*28*, *32*), implying that the chromophore and its binding pocket are not significantly affected by crystal packing. The high-resolution structure of the CBD of *Dr*BphP suggests an exocyclic extension of the π-conjugation system at ring A of the BV chromophore by rearrangement of the double bond from C2=C3 to C3=$C3^1$, leading to the same electronic configuration at ring A as in unbound PCB and PϕB (*30*). The planes of rings A and D are tilted by 15° and 44°, respectively, relative to that of the nearly coplanar rings B and C (*30*). The chromophore is embedded in a hydrogen-bonded network including two highly conserved aspartic acid and histidine residues (D207 and H260 in *Dr*BphP) that are essential, at least in the closely related Agp1, for the stabilization of the protonated chromophore structure in the P_r state (*33*).

Quite recently, the first three-dimensional (3D) structure of the cyanobacterial phytochrome Cph1 in the P_r state that includes the PHY domain and is missing only the histidine kinase domain was determined (*34*). The PCB chromophore is attached to Cys259 in the GAF domain and adopts a $5Z_{syn},10Z_{syn},15Z_{anti}$ configuration/conformation as predicted from heteronuclear NMR investigations of the same protein (*35*). The geometry of the PCB chromophore is thus analogous to that of BV in bacteriophytochromes, although it is clearly less twisted (*34*). The structure of the complete sensory module of Cph1 reveals a tonguelike protrusion from the PHY domain that seals the chromophore pocket from solvent access and is probably important in signal transmission. Almost the same arrangement of the PAS, GAF, and PHY domains was found in the crystal structure of the photosensory core domain of the bacteriophytochrome *Pa*BphP in its dark-adapted P_{fr}-enriched state (*36*). The structure of *Pa*BphP provides for the first time crystallographic information about the P_{fr} state and identifies key interactions of the GAF−PHY interface that stabilize the chromophore in this state. The geometry of the BV chromophore could not be determined unambiguously; however, data refinement clearly favors the

$5Z_{syn}$,$10Z_{syn}$,$15E_{anti}$ configuration (*36*). The $15E_{anti}$ configuration has already been predicted from assembly studies of Agp1 with locked BV derivatives, suggesting that the C−D methine bridge remains in the *anti* conformation during photoconversion (*28*). In contrast, the locked $5Z_{syn}$ adduct of Agp1 did not exhibit a P_{fr}-like photoproduct, implying a conformational change in the A−B methine bridge upon photoconversion (*32*). Flash photolysis experiments with this adduct suggested that the putative conformational change of the A−B methine bridge occurs in the Meta-R_A to Meta-R_C transition of the thermal relaxation cascade (*37*). The actual stereochemistry of the A−B methine bridge of the BV chromophore in the P_{fr} state of bacteriophytochromes remains to be determined. The $5Z_{syn}$,$10Z_{syn}$,$15E_{anti}$ configuration was assigned to the PCB chromophore in the P_{fr} state of Cph1 on the basis of heteronuclear NMR investigations (*35*).

In this work, we use circular dichroism and time-resolved absorption spectroscopy to study the spectral and kinetic properties of covalent and noncovalent bilin adducts of Agp1 phytochrome from *Agrobacterium tumefaciens* with the goal of understanding the role and function of the covalent attachment. Circular dichroism is a measure of the chirality (twisting) of the chromophore and reflects the nonplanarity of the chromophore geometry. Utilization of the two bilin chromophores, BV and PCB, and appropriate variants of Agp1 allows the preparation of covalent and noncovalent adducts with both chromophores: Agp1−BV (covalent), Agp1-C20A−BV (noncovalent), Agp1−PCB (noncovalent), and Agp1-V249C−PCB (covalent). Unexpectedly, deletion of the N-terminal peptide segment including amino acids 2−19 also prevents covalent attachment of BV to Cys20.

We found that the CD spectra of the P_r forms of all adducts are qualitatively the same. In the CD spectra of the P_{fr} forms, the covalent PCB adduct exclusively displays the well-known sign reversal of the Q-band described for plant phytochromes (*38*, *39*) and Cph1 (*24*) and attributed to the $Z-E$ isomerization of the C−D methine bridge. In the three other adducts, the Q-band CD is almost zero, suggesting a contribution from an out-of-plane rotation of the A ring of the chromophore that leads to an apparent compensation by the more extended π-conjugation system, including ring A. This contribution is absent or strongly reduced in the shorter π-conjugation system of the covalent PCB adduct. Flash photolysis measurements with these adducts demonstrated that both the kinetics and the spectral characteristic of the P_r to P_{fr} photoconversion are not substantially affected by the covalent attachment. We conclude that covalent attachment of the bilin chromophore is not required for the spectral and functional integrity of the Agp1 phytochrome. However, the noncovalent BV adducts (C20A and Δ18N) are much more sensitive to photobleaching than the covalent BV adduct, implying that the covalent attachment provides a considerable stabilization of the chromophore. In the PCB adducts, the formation of P_{fr} is accelerated by 2 orders of magnitude with respect to the BV adducts of Agp1. Nevertheless, the spectral signature of the photoconversion in the PCB adducts is quite similar to that in the BV adducts but clearly distinct from that of Cph1. The relaxation pathway after photoisomerization is thus governed by specific protein−cofactor interactions rather than by the chemical structure of the chromophore and the type of attachment.

MATERIALS AND METHODS

Protein Expression, Purification, and Assembly. Five different variants of *Agrobacterium* phytochrome Agp1 that were expressed in *Escherichia coli* were used in this study. The cloning of the expression vectors and details for purification were given in earlier publications (*12*, *40*, *41*). Agp1 is the wild-type full-length protein (see Figure 1B). In Agp1-C20A, the chromophore binding Cys20 is replaced by an Ala. Agp1-M15 contains the 504 N-terminal amino acids of Agp1, including the PAS, GAF, and PHY domains, but lacks the C-terminal histidine kinase. Agp1-M15Δ18N is similar to Agp1-M15, but 18 N-terminal amino acids (Gln2−Ser19) are lacking. In Agp1-V249C, a cysteine was introduced into the GAF domain allowing PCB to bind covalently at its canonical position (*13*). All proteins carry a C-terminal polyhistidine tag for affinity purification. In general, the phytochromes were purified as apoproteins. To obtain holoprotein, the BV and PCB chromophores from ~5 mM DMSO or methanol stock solutions were added at an ~1.5-fold molar excess. After incubation for >1 h, the sample was passed through a NAP-10 desalting column (GE Healthcare) which had been equilibrated with basic buffer.

Assay for Covalent Binding. For assays of covalent binding, the assembled holoprotein was diluted with basic buffer so that the A_{280} was approximately 1. A NAP-10 column was equilibrated with basic buffer that contained 1% SDS. To 900 μL of protein solution was added 100 μL of SDS from a 10% aqueous stock solution. This treatment denatures the protein and dissociates the noncovalently bound chromophore. One milliliter of the protein/SDS solution was passed through the NAP column, and 1.5 mL of the flow through was collected. Absorption spectra before and after NAP column separation were normalized to A_{280}. Covalent binding is indicated by the absorbance of the coeluted chromophore in the visible spectral range (*12*, *13*, *28*).

Circular Dichroism Spectroscopy. Stationary CD spectra were recorded with a Jasco 500A instrument modified and updated with a homemade data acquisition system (*24*, *42*). By using a fixed slit (100 μm) at the outlet of the monochromator, the signal-to-noise ratio in the far-red range could be significantly improved. Because of the dispersion of the prism monochromator, the spectral bandwidth decreased continuously from 7.5 nm at 800 nm to 0.4 nm at 300 nm. Artifacts from photoconversion due to the measuring light have not been observed. Data were collected at room temperature, with cells with a path length of 10 mm, and averaged over 10−15 scans. For baseline corrections, reference spectra recorded with buffer were subtracted.

Calculation of Pure Pr and Pfr Spectra. CD and absorption spectra of the pure P_r and P_{fr} forms were extrapolated from the respective spectra after red light and far-red light illumination (or dark reversion), respectively, by variation of the estimated relative contributions of P_r and P_{fr} in the mixed states. Empirical constraints on the shape of the spectra were used, e.g., preclusion of negative absorption, shoulder at the blue edge of the Q-bands, etc. The experimental spectra are shown together with the calculated P_r and P_{fr} spectra in the Supporting Information (Figures S1−S3). The good agreement of the P_{fr} spectra of Agp1 (calculated) and Agp2 (measured) in the Q-band range corroborates the empirical approach for the calculation of the P_{fr} spectra of Agp1 (Figure S2).

Transient Absorption Spectroscopy. Flash photolysis was performed as described previously (*20*, *21*). Absorbance changes with respect to the P_r state were recorded after laser flash excitation at 695 or 640 nm by using the emission of appropriate laser dyes pumped by an excimer laser (RD-EXC-100, Radiant Dyes Laser&Accessories GmbH). Before each flash excitation, the sample was reconverted with far-red light to the P_r state.

For the BV adducts of Agp1, this was achieved by a 20 s illumination with a 784 nm laser diode (RLD78PZW2, Laser Components) operated at a power of 60 mW. For the PCB adducts of Agp1, reconversion was achieved with a 10 s illumination with a 150 W tungsten halogen fiber lamp (KL1500, Schott) filtered through a high-pass filter (RG715/RG9). Time traces at multiple wavelengths were analyzed by singular-value decomposition (SVD). The traces of the relevant SVD components were fitted simultaneously with a sum of exponentials. Amplitude spectra were calculated from the amplitudes of these fits and the related SVD basis spectra as described previously (*24*). The extrapolated initial difference spectra (ΔA_{init}) were calculated by adding amplitude spectra B_0, B_1, B_2, ..., B_i. Photoinduced proton release and uptake processes were monitored by using appropriate pH indicator dyes as described previously (*20*, *21*, *43*). To minimize the contribution from the bilin chromophore to the dye signal, cresol red (λ_{max} = 570 nm) was used for the BV adducts and pyranine (λ_{max} = 455 nm) for the covalent PCB adduct. For sufficient sensitivity, the dye measurements were perfomed at pH values close to the respective pK_a values of 8.2 (cresol red) and 7.2 (pyranine).

RESULTS

Circular Dichroism Spectra of BV Adducts. Absorption and CD spectra of the P_r and P_{fr} forms of Agp1-WT (covalent BV adduct) and Agp1-C20A (noncovalent BV adduct) are shown in Figure 2. The CD spectrum of the P_r form of Agp1-WT (Figure 2B) is very similar to that of the P_r forms of plant phytochromes (*38*, *39*) and the cyanobacterial phytochrome Cph1 (*24*). The Q-band (λ_{max}~700 nm) displays a strong negative CD signal, while in the Soret range (λ_{max} ~ 390 nm), the CD is positive with approximately the same magnitude. The molar ellipticity of the Q-band of Agp1-WT in the P_r form is approximately the same as that of plant phytochrome [$\sim 3 \times 10^5$ deg cm^2 dmol^{-1} (*39*)] and by a factor of ~2 larger than that of cyanobacterial phytochrome (*24*). The CD spectrum of the P_{fr} form of Agp1-WT (Figure 2B) differs significantly from that of plant and cyanobacterial phytochromes where the CD of the Q-band reverses sign upon photoconversion (*24*, *38*, *39*). In Agp1-WT, this reversal is absent and a rather weak negative CD band remains in P_{fr} at ~750 nm, the λ_{max} of the absorption in the Q-band. However, the CD of the P_{fr} form of Agp1-WT in the Soret range, including two weak positive bands at ~430 and 360 nm, is similar to that of plant phytochrome.

The BV adduct of Agp1-C20A displays wild-type-like photochromicity, though the chromophore is noncovalently attached (*4*). For direct comparison, the absorption spectra of Agp1-WT were scaled to approximately the same absorption of the P_r state at 700 nm (Figure 2A). The absorption spectra of the P_r and P_{fr} states of Agp1-C20A are characterized by larger spectral widths and smaller ratios of the Q-band to the Soret band absorption with respect to Agp1-WT (Figure 2A). The overall shape of the CD spectrum of the P_r form of Agp1-C20A is the same as that of Agp1-WT (Figure 2B), suggesting that the covalent attachment of the BV chromophore does not affect its geometry substantially. However, in Agp1-C20A, the ratio of the ellipticities of the Q-band and the Soret band differs significantly from that of Agp1-WT (1:2 vs 1:1). Moreover, the absolute value of the ellipticity in Agp1-C20A is much smaller than in Agp1-WT [~$^2/_3$ in the Soret band and ~$^1/_3$ in the Q-band with respect to Agp1-WT (see Figure 2B)] in the P_r form. From the comparison

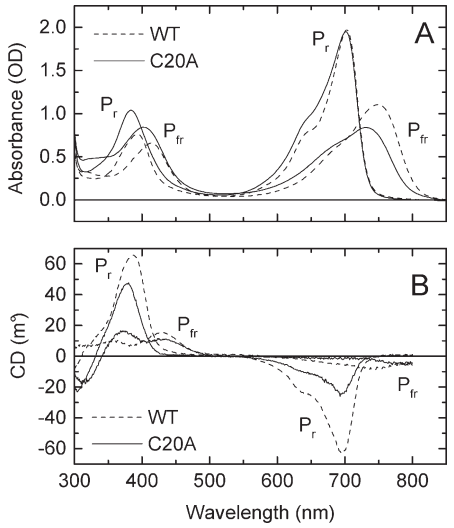

FIGURE 2: Absorption (A) and CD (B) spectra of the BV adducts of Agp1-WT (---) and Agp1-C20A (—). The spectra of the P_r and P_{fr} states are labeled accordingly. The P_r and P_{fr} spectra were calculated from the spectra after red light and far-red light illumination (see Materials and Methods). Absorption and CD spectra were measured with path lengths of 5 and 10 mm, respectively, and the former were scaled to a path length of 10 mm. The absorption spectra were scaled to approximately the same absorption of the P_r state at 700 nm. The same scaling factors were used for the CD spectra.

of the CD spectra of the covalent (Agp1-WT) and noncovalent (Agp1-C20A) BV adducts, we conclude that in Agp1 the formation of the covalent bond is accompanied by a strong increase in the ellipticity of the Q-band. The CD spectrum of the P_{fr} form of Agp1-C20A displays the same features as and rotational strengths comparable to those of Agp1-WT (Figure 2B). Minor differences were observed in the relative intensities and positions of the bands in the Soret range. Blocking of cysteine 20 in Agp1-WT by IAA or DTNB and successive regeneration with BV lead to CD spectra in both the P_r and P_{fr} forms that are almost identical to those of the BV adduct of Agp1-C20A (data not shown).

The absorption and CD spectra of the BV adduct of Agp1-M15Δ18N revealed striking agreement with that of Agp1-C20A in both the P_r and P_{fr} forms (Figure S4, Supporting Information). Difference spectra taken from dark reversion after red light illumination (Figure S4B) barely allow us to distinguish between Agp1-C20A (solid line) and Agp1-M15Δ18N (dotted line). Both differ significantly from the difference spectrum of Agp1-WT (dashed line in Figure S4B) by a smaller and blue-shifted Q-band absorption of the P_{fr} form and a blue shift of the Soret bands. The small differences in the CD spectra of Agp1-C20A and Agp1-M15Δ18N (Figure S4C) are negligible compared to the huge differences with respect to Agp1-WT. We note that no significant differences in the absorption and CD spectra were observed between the BV adducts of Agp1-WT (full-length) and Agp1-M15-WT that lacks the C-terminal His kinase (data not shown).

Circular Dichroism Spectra of PCB Adducts. Absorption and CD spectra of the P_r and P_{fr} forms of the PCB adducts of Agp1-M15-WT (noncovalent) and Agp1-V249C (covalent) are shown in Figure 3. In contrast to the BV adducts, the absorption spectra of the P_r forms of the covalent and noncovalent PCB adducts differ in the position of their Q-band maxima by ~30 nm [655 and 685 nm for the covalent and noncovalent PCB adduct, respectively (see Figure 3A)]. This blue shift is due to the saturation of the ring A ethylidene double bond of PCB upon

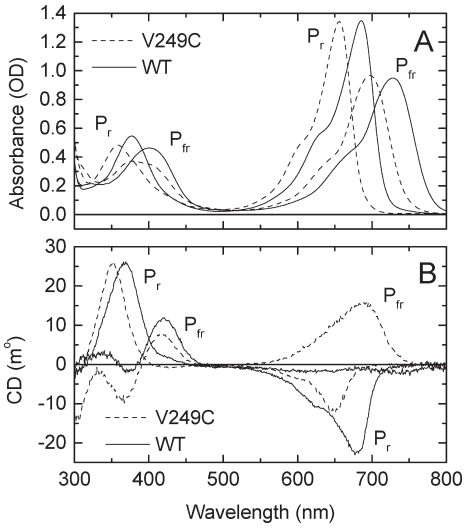

FIGURE 3: Absorption (A) and CD (B) spectra of the PCB adducts of Agp1-M15-WT (—) and Agp1-V249C (---). The spectra of the P_r and P_{fr} states are labeled accordingly. The P_r and P_{fr} spectra were calculated from the spectra after red light and far-red light illumination (see Materials and Methods). Absorption and CD spectra were measured with path lengths of 5 and 10 mm, respectively, and the former were scaled to a path length of 10 mm. The absorption spectra were scaled to approximately the same absorption of the P_r state at the maximum of the main absorption band. The same scaling factors were used for the CD spectra.

covalent attachment (*13*, *24*) and is also present in the CD spectra. The CD spectra of the noncovalent PCB adduct (Agp1-M15-WT, solid lines in Figure 3B) show striking similarities with those of the covalent BV adduct: (i) the ratio of the ellipticities of the Q-band and the Soret band is ~1:1 in the P_r state, and (ii) the ellipticity of the Q-band reaches almost zero upon photoconversion to the P_{fr} state. In contrast, the CD spectra of the covalent PCB adduct (Agp1-V249C, dashed lines in Figure 3B) reveal remarkable differences with respect to those of the noncovalent PCB adduct. The ratio of the ellipticities of the Q-band and the Soret band is ~1:2 in the P_r state of the covalent PCB adduct. Provided that the scaling of the absorption spectra (Figure 3A) reflects equal concentrations, the ellipticity of the Soret band in the P_r state is the same in the covalent and noncovalent PCB adducts, while the ellipticity of the Q-band is reduced by ~$^1/_2$ in the covalent PCB adduct. Upon photoconversion to the P_{fr} state, the CD of the Q-band of the covalent PCB adduct displays sign reversal as observed with the (covalent) PCB adduct of Cph1 (*24*) and with plant phytochromes (*38*, *39*). The pattern in the Soret range of the CD spectra of the P_{fr} forms of the covalent and noncovalent PCB adducts is very similar, however, and is clearly more pronounced than in the CD spectra of the P_{fr} forms of the BV adducts (see Figures 2B and 3B). Apart from the relative amplitudes of the contributing bands, the CD spectra of the covalent PCB adducts of Agp1 (dashed lines in Figure 3B) and Cph1 (Figure 10A of ref (*24*)) are compatible.

Photoconversion Kinetics and Protonation Changes of BV Adducts. Flash photolysis was performed with the BV adducts of Agp1-M15-WT, Agp1-C20A, and Agp1-M15Δ18N under the same conditions. In Figure 4A, time traces from these samples at the three characteristic wavelengths, 700, 725, and 750 nm, are shown. Just like the spectra of the P_r and P_{fr} forms, the kinetics of the covalent BV adducts of full-length and M15 are almost indistinguishable. Since Agp1-C20A and Agp1-M15Δ18N suffered from photobleaching, the related traces were corrected

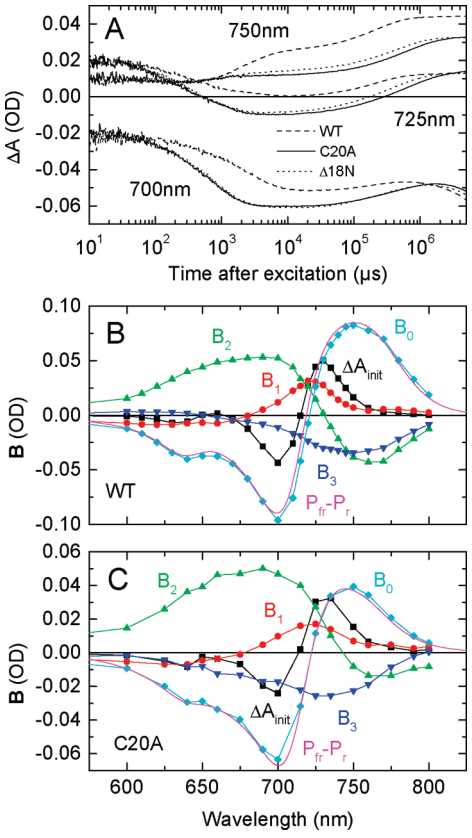

FIGURE 4: (A) Flash-induced absorption changes of the BV adducts of Agp1-M15-WT (---), Agp1-C20A (—), and Agp1-M15Δ18N (···) measured at 700, 725, and 750 nm. The traces of Agp1-C20A and Agp1-M15Δ18N were corrected for irreversible bleaching and scaled to match the initial (~10 μs) absorption changes of Agp1-M15-WT. The three traces of each sample were scaled with the same factor. Conditions: 20 mM Tris, 50 mM NaCl, pH 7.8, 20 °C. (B and C) Amplitude spectra of Agp1-M15-WT and Agp1-C20A, respectively. ΔA_{init} is the sum of amplitude spectra B_0−B_3. The magenta lines are the steady-state P_{fr} − P_r difference spectra scaled to the B_0 spectra.

by rescaling to the linearly extrapolated initial (unbleached) state. For the sake of comparison, the traces of Agp1-C20A and Agp1-M15Δ18N were further scaled to match the initial (~10 μs) absorption changes of Agp1-M15-WT. The latter scaling mainly accounts for different concentrations of the chromoprotein and different excitation energies. We note that the excitation efficiency is almost the same in the mutants and in WT, indicating that the quantum yields of the corresponding P_r states are very similar. The kinetics of Agp1-C20A and Agp1-M15Δ18N are barely distinguishable but differ significantly from that of Agp1-M15-WT. Simultaneous fits with three exponentials to traces at eight wavelengths [380, 420, 650, 675, 700, 725, 735, and 750 nm (data not shown)] revealed a decrease in the time constant of the second component (formation of Meta-R_C) by a factor of 3−4 in the mutants [2.8 ms in Agp1-M15-WT vs 940 μs in Agp1-M15Δ18N and 740 μs in Agp1-C20A (see Table 1)]. The deviations between the traces of WT and the mutants also arise from differing amplitudes, in particular from those of the second transition, as illustrated by the amplitude spectra of Agp1-M15-WT (Figure 4B) and Agp1-C20A (Figure 4C). However, each amplitude spectrum of WT has its counterpart with similar spectral characteristics in the mutants (B_0−B_3 of Figure 4B,C). The extrapolated initial difference spectrum ΔA_{init} ($\sum_{i=0} B_i$) reflecting the Lumi-R minus P_r difference spectrum is almost the same in the WT and mutants. The transitions related to amplitude

Table 1: Kinetics of the P_r to P_{fr} Photoconversion of the BV Adducts of Agp1[a]

	τ_1, Lumi-R → Meta-R_A	τ_2, Meta-R_A → Meta-R_C	τ_3, Meta-R_C → P_{fr}
Agp1-M15-WT	280 μs	2.8 ms	220 ms
Agp1-M15Δ18N	230 μs	940 μs	290 ms
Agp1-C20A	120 μs	740 μs	360 ms

[a] Time constants from simultaneous fits with three exponentials to traces at eight wavelengths (380, 420, 650, 675, 700, 725, 735, and 750 nm). Conditions: 20 mM Tris, 50 mM NaCl, pH 7.8, 20 °C.

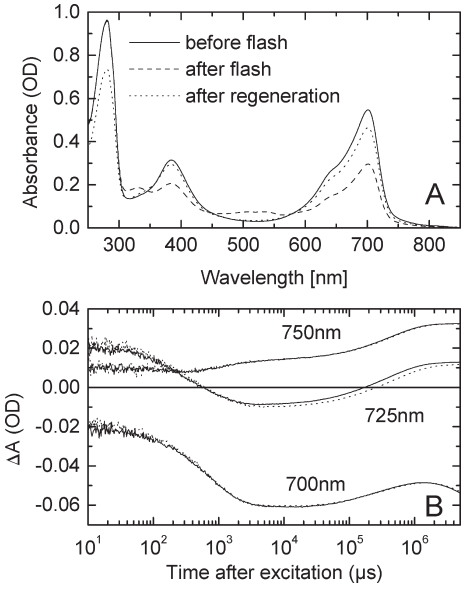

FIGURE 5: (A) Absorption spectra of the BV adduct of Agp1-M15Δ18N before (—) and after (---) the flash measurements and after regeneration with fresh BV and elution from a desalting column (···). (B) Flash-induced absorption changes of Agp1-M15Δ18N before (—) and after (···) regeneration with fresh BV. The traces of the regenerated sample were scaled to the same initial absorption changes.

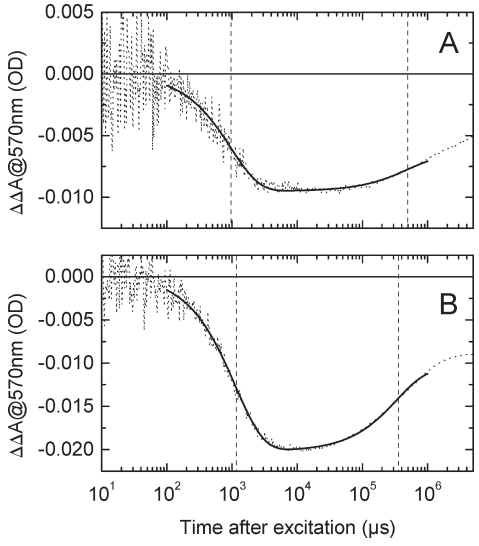

FIGURE 6: Protonation signals of the BV adducts of Agp1-C20A (A) and Agp1-M15Δ18N (B) (···) calculated from traces measured at 570 nm with (100 μM) and without cresol red. Conditions: unbuffered, 50 mM NaCl, pH 7.8, 20 °C. The protonation signals were fitted simultaneously with the traces measured at 750 nm (Agp1-C20A) and 700 nm (Agp1-M15Δ18N), respectively, to a sum of three exponentials. Only two components were required to fit the protonation signals (thick solid lines). The related time constants of proton release and proton uptake are marked by dashed vertical lines: 960 μs and 490 ms for Agp1-C20A and 1.1 and 340 ms for Agp1-M15Δ18N, respectively.

spectra B_1-B_3 of Agp1-C20A were thus assigned to the decays of Lumi-R-, Meta-R_A-, and Meta-R_C-like intermediates. Absorption spectra of Agp1-M15Δ18N before and after flash photolysis measurements (110 flashes) are shown in Figure 5A (solid and dashed lines, respectively). The Q-band of the chromophore is bleached by almost 50%. The increase in absorption in the range from 450 to 550 nm may be interpreted as the formation of BV photoproducts exhibiting a shorter π-conjugated system. Very similar spectra were observed upon photobleaching with Agp1-C20A (data not shown). When fresh BV is added to the bleached Agp1-M15Δ18N sample, the Q-band absorption recovers, suggesting that BV displaces the photobleached BV from the binding pocket. After elution from a desalting column to remove excess chromophore, the spectrum is again very similar to the initial one (dotted vs solid line in Figure 5A), indicating an almost complete regeneration. Flash photolysis measurements show that the kinetics of the P_r to P_{fr} photoconversion of the regenerated adduct are the same as that of the holoprotein (see Figure 5B). These experiments show that photobleaching exclusively affects the cofactor and leaves the chromophore binding pocket intact.

Proton transfer to the aqueous medium was studied with the mutants Agp1-C20A and Agp1-M15Δ18N by using the pH indicator dye cresol red. As already demonstrated for Agp1-WT (*21*), sequential proton release and proton uptake components were observed with both mutants (Figure 6). Since the amplitude of the uptake component is smaller than that of the release component, the photoconversion is accompanied by a net acidification. Kinetically, proton release and uptake are associated with the second and third transition, respectively, that were resolved in the photoinduced relaxation cascade and that were attributed in Agp1-WT to the formation of Meta-R_C and P_{fr}, respectively. From simultaneous fits with traces measured at 750 nm (Agp1-C20A) and 700 nm (Agp1-M15Δ18N), time constants of 960 μs and 490 ms for Agp1-C20A (Figure 6A) and 1.1 and 340 ms for Agp1-M15Δ18N (Figure 6B), respectively, were determined. These numbers differ slightly from those of Table 1 (τ_2 and τ_3) probably because of the absence of buffer in the dye experiment. Consistent with the acceleration of the formation of Meta-R_C in both mutants described above, proton release is also accelerated by a factor of ~3 with respect to that of WT. The kinetics of P_{fr} formation and partial proton uptake are not significantly affected by the mutations. The close kinetic coupling of spectral transitions of the chromophore and proton transfer to the solvent is thus maintained in the mutants.

Photoconversion Kinetics and Protonation Changes of PCB Adducts. Flash photolysis was performed with the PCB adducts of Agp1-M15-WT and Agp1-V249C at multiple wavelengths under the same conditions. For direct comparison of the kinetics of the covalent and noncovalent PCB adducts, time

traces at three characteristic wavelengths are shown in Figure 7A. The choice of these wavelengths, 680, 705, and 730 nm for Agp1-M15-WT (solid lines in Figure 7A) and 655, 675, and 700 nm for Agp1-V249C (dashed lines in Figure 7A), takes into account the blue shift in the spectra of the covalent PCB adduct. The traces of Agp1-M15-WT were scaled to match the initial (~10 μs) absorption changes of Agp1-V249C at the absorption maxima of the corresponding P_r and P_{fr} states. Due to the high photostability of the PCB adducts, traces at multiple wavelengths from the near UV to the far red could be measured, and only minor corrections for irreversible bleaching were necessary. The time traces at the characteristic wavelengths show that the kinetics of the PCB adducts of Agp1-M15-WT (noncovalent) and Agp1-V249C (covalent) are very similar. Interestingly, the major absorption changes at these wavelengths occur in the time range below 10 ms, implying that the kinetics of P_{fr} formation in the PCB adducts of Agp1 is much faster than in the BV adducts. SVD analysis of data sets including time traces at multiple (at least 32) wavelengths revealed four relevant spectral components for both adducts. Simultaneous fits with four exponentials to the related SVD traces afforded time constants of 82 μs, 620 μs, 3.9 ms, and 85 ms for Agp1-M15-WT and 130 μs, 720 μs, 1.9 ms, and 20 ms for Agp1-V249C (see Table 2). The corresponding five amplitude spectra, B_0−B_4, and the extrapolated initial difference spectra, ΔA_{init}, are similar in both PCB adducts (Figure 7B,C) and display the same overall spectral characteristics as those of the BV adducts (Figure 4B,C). The amplitudes of the fourth transition in the photoconversion of the PCB adducts (amplitude spectra B_4 in Figure 7B,C) are very small and moreover limited to the neighborhood of the absorption maximum of the respective P_{fr} state. This transition probably does not reflect the presence of an additional species with respect to the photoconversion of the BV adducts. However, fits with only three exponentials led to multimodal amplitude spectra B_2 and B_3 that could not be interpreted consistently. The amplitude spectra B_0 (light blue symbols in Figure 7B,C), the extrapolated final difference spectra, are in good (Agp1-M15-WT) to perfect (Agp1-V249C) agreement with the stationary P_{fr} minus P_r difference spectra (solid magenta lines), supporting complete P_{fr} formation within the considered time window. While the extrapolated initial difference spectra, ΔA_{init}, and the amplitude spectra, B_1, of both PCB adducts are almost the same, amplitude spectra B_2 and B_3 show only rough agreement. Intriguingly, B_2 and B_3 of the noncovalent PCB adduct [Agp1-M15-WT (Figure 7B)] are more similar to their counterparts of the covalent BV adduct [Agp1-M15-WT (Figure 4B)], reflecting the Meta-R_A to Meta-R_C and Meta-R_C to P_{fr} transitions, respectively. B_2 of the covalent PCB adduct displays smaller amplitudes and a smaller red shift (V249C, Figure 7C), while the amplitudes of B_3 are larger than those of the noncovalent PCB adduct and describe a further substantial red shift. B_3 of the noncovalent PCB and covalent BV adducts is mainly associated with an absorption increase of the Q-band (negative amplitudes) in the formation of P_{fr}. Since amplitude spectra B_4 of the PCB adducts contribute only little to the formation of the final photoproduct, P_{fr}, the predominant fraction of P_{fr} is formed in the third transition with time constants of 3.9 and 1.9 ms, respectively.

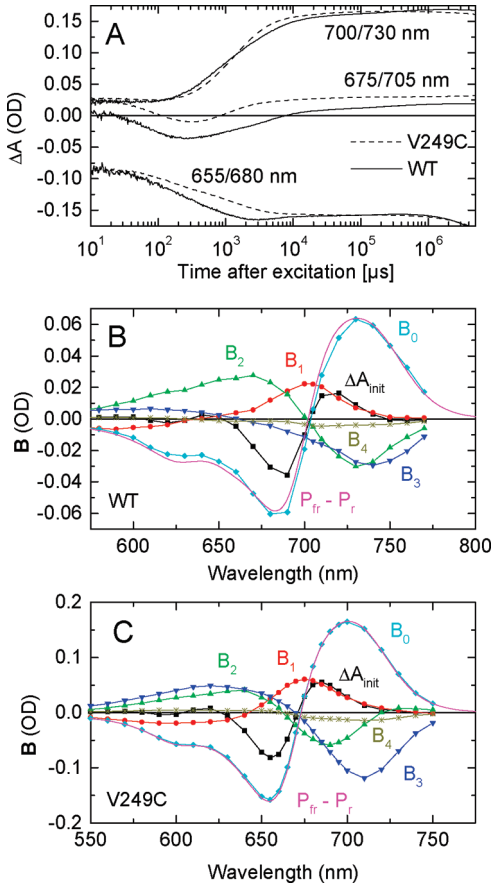

FIGURE 7: (A) Flash-induced absorption changes of the PCB adducts of Agp1-M15-WT measured at 680, 705, and 730 nm (—) and Agp1-V249C measured at 655, 675, and 700 nm (---). The traces of Agp1-M15-WT were scaled to match the initial (~10 μs) absorption changes of Agp1-V249C. The three traces of each sample were scaled with the same factor. Conditions: 50 mM Tris, 200 mM NaCl, pH 7.8, 20 °C. (B and C) Amplitude spectra of the PCB adducts of Agp1-M15-WT and Agp1-V249C, respectively, in the Q-band range. The range of the Soret bands has been omitted for the sake of clarity. ΔA_{init} is the sum of amplitude spectra B_0−B_4. The magenta lines are the steady-state P_{fr} − P_r difference spectra scaled to the B_0 spectra.

To detect proton transfer to the external medium and its stoichiometry with the covalent PCB adduct (Agp1-V249C), the pH indicator dye pyranine was added to the unbuffered solution (pH 7.0) at different concentrations (0, 40, 80, 160, and 240 μM). Transient absorption changes were measured at 455 nm, the absorption maximum of the deprotonated species of the dye, and at the three characteristic wavelengths of the covalently bound PCB chromophore, 655, 675, and 700 nm. The protonation signal shows only an apparent release component in the time range

Table 2: Kinetics of the P_r to P_{fr} Photoconversion of the PCB Adducts of Agp1[a]

	τ_1, Lumi-R → Meta-R_A	τ_2, Meta-R_A → Meta-R_C	τ_3, Meta-R_C → P_{fr}	τ_4
Agp1-M15-WT	82 μs	620 μs	3.9 ms	85 ms
Agp1-V249C	130 μs	720 μs	1.9 ms	20 ms

[a] Time constants from simultaneous fits with four exponentials to the four relevant SVD traces obtained from SVD of time traces at multiple wavelengths in the ranges of 360−770 nm (Agp1-M15-WT) and 340−750 nm (Agp1-V249C). Conditions: 50 mM Tris, 200 mM NaCl, pH 7.8, 20 °C.

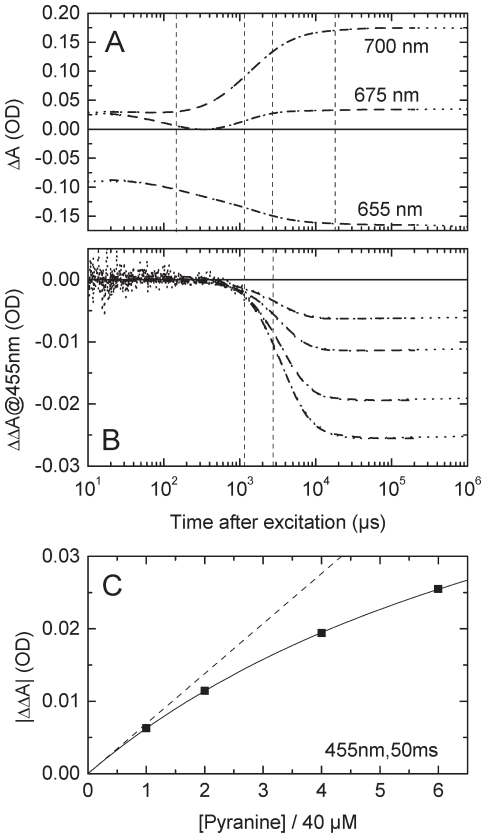

FIGURE 8: (A) Flash-induced absorption changes of the PCB adduct of Agp1-V249C measured at 655, 675, and 700 nm in an unbuffered solution (200 mM NaCl, pH 7.0, 20 °C) in the presence of the pH indicator dye pyranine (average of the traces at 0, 40, 80, 160, and 240 μM pyranine). (B) Protonation signals of the PCB adduct of Agp1-V249C (···) calculated from the traces measured at 455 nm with (40, 80, 160, and 240 μM) and without pyranine. The thick dashed lines result from a simultaneous fit with four exponentials to the traces of panels A and B. The dashed vertical lines mark the corresponding time constants. In panel B, the amplitudes of the first and fourth components are negligible and the corresponding vertical lines have thus been omitted. (C) Absolute value of the dye signal at different dye concentrations read from the traces at 50 ms in panel B. The solid line is a fit of the data to eq 1 of ref (*44*) with $\Delta\Delta A(f\rightarrow\infty) =$ 66 mOD. The dashed line is the predicted dependence in the absence of saturation effects.

of milliseconds, whereas a reuptake component is absent (Figure 8B). The chromophore signals indicate that the kinetics was unaffected by the concentration of the dye (data not shown), allowing the use of averaged time traces (see Figure 8A) for further analysis. The protonation signals at the four measured concentrations of pyranine (see Figure 8B) and the averaged traces reflecting the chromophore were fitted simultaneously with a sum of four exponentials. Time constants of 140 μs, 1.1 ms, 2.7 ms, and 18 ms were obtained from this fit, in good agreement with the results from the global analysis described above. The minor differences may be due to a slightly lower pH value, the absence of buffer, and the limited number of traces in the dye measurements. The amplitudes of the fit show that the protonation signal is associated exclusively with the second (1.1 ms) and third (2.7 ms) kinetic component. However, these amplitudes exhibit opposite signs, leading to an apparent over-exponential rise of the protonation signal; i.e., the rise is steeper than that of a single exponential (see Figure S5 of Supporting Information). The expected sequence of proton release and partial reuptake is apparently obscured by the very small difference between the two time constants. To determine the concentration of the net proton release, the dye signal at ~50 ms was extrapolated to an infinite dye concentration by fitting a saturation curve according to eq 1 of ref (*44*) to the data points at different dye concentrations (Figure 8C). From the extrapolated value of 0.066 ± 0.007 optical density unit with a path length of 0.5 cm and an extinction coefficient of pyranine at 455 nm of 24000 M^{-1} cm^{-1}, a concentration of released protons of 5.5 ± 0.6 μM was obtained. Using an estimated difference of the extinction coefficients of P_r and P_{fr} at 700 nm ($\Delta\varepsilon$) of 55000 ± 5000 M^{-1} cm^{-1} (*4*), the absorption change at ~100 ms measured at 700 nm reflects a concentration of photoconverted molecules of 6.4 ± 0.7 μM. The stoichiometry of net proton release is thus 0.9 ± 0.2.

Demonstration of Noncovalent Adduct Formation in Δ18N. The goal of this work was to characterize covalent and noncovalent bilin adducts of Agp1. Since the N-terminal domain is potentially involved in the covalent attachment of the BV chromophore at Cys20 in Agp1, the Agp1-M15Δ18N mutant (see ref (*40*)) was included in our studies. During the course of our spectroscopic measurements, several indications that this mutant might also incorporate the chromophore in a noncovalent manner emerged. We therefore performed SDS desalting column separation with M15Δ18N, an assay that has been established for testing covalent chromophore attachment in several cases (*12*, *28*). Estimating from the normalized absorbance spectra, we found only ~10% of the originally assembled chromophore eluted together with the protein in the front fraction (Figure S6, Supporting Information). Previous studies have shown that ca. 7% of the chromophores appear in the front fraction, if the assay is performed without protein (*12*). Therefore, either the major portion or all of the chromophore is noncovalently bound to Agp1-M15Δ18N, despite the presence of Cys20, to which BV binds in the wild-type protein.

DISCUSSION

Geometry of the Bilin Chromophore in the P_r and P_{fr} Forms. In this study, the P_r and P_{fr} forms of covalent and noncovalent bilin adducts of Agp1 phytochrome were characterized by CD spectroscopy. The P_r forms of all four adducts exhibit the same spectral pattern, including negative ellipticity in the Q-band and positive ellipticity in the Soret band of approximately the same order of magnitude as already reported for plant phytochromes (*38*, *39*), the cyanobacterial phytochrome Cph1 (*24*), the bacteriophytochrome *Dr*BphP, and a P_r-like mutant of the cyanobacteriochrome Tlr0924 (*45*). The qualitative agreement of the CD spectra of the P_r forms suggests that the conformations and configurations of the different bilin chromophores (PCB, PϕB, and BV) as well as the facial dispositions of the A and D rings (see the conceptual model introduced in ref (*45*)) are the same in all of these species. Indeed, the recent X-ray diffraction and NMR investigations of the structure of Cph1 revealed that the PCB chromophore adopts the *ZZZssa* configuration in the P_r form (*34*, *35*) as BV does in the bacteriophytochromes *Dr*BphP (*29*, *30*) and *Rp*BphP3 (*31*). It is thus very unlikely that the configuration of the PϕB chromophore in the P_r form of plant phytochrome is *ZZZasa* as concluded from RR spectroscopy (*46*).

The type of covalent attachment involving either an ethylidene group (PCB and PϕB) or a vinyl group (BV) at the C3 atom of the chromophore and the respective electronic configuration at ring A are apparently of minor importance for the characteristic

pattern of the CD bands of the P_r forms. Since the CD spectra of the noncovalent BV and PCB adducts of Agp1 in the P_r state are very similar to those of the corresponding covalent adducts, a change in the chromophore configuration upon covalent attachment is unlikely, implying that the configuration of the noncovalently bound bilin chromophores is also *ZZZssa* in the P_r state. Recent time-dependent density functional theory (TDDFT) calculations on model compounds mimicking the PCB chromophore in the P_r state of Cph1 showed that reasonable wavelength maxima for the two main absorption bands and the correct signs of the corresponding ellipticities could only be obtained for the *Z,syn* configuration of the A−B methine bridge and α-facial disposition of the ring D nitrogen relative to the B/C ring system (*45*).

Apart from the qualitative agreement of the CD spectra of the P_r forms, the ratios of the ellipticities of the Q-band and the Soret band of the noncovalent adducts and their absolute values differ considerably from those of the covalent adducts. Interestingly, the ratio of the ellipticities is ∼1:1 in the P_r forms of the covalent BV adduct and the noncovalent PCB adduct, while it is ∼1:2 in the P_r forms of the noncovalent BV adduct and the covalent PCB adduct. The agreement of this ratio in the P_r forms of the covalent BV adduct and the noncovalent PCB adduct may be due to the same electronic configuration at the A ring of the chromophores, including an exocyclic extension of the π-conjugation system at the C3 atom (*30*). In contrast, the agreement of the lower ratio of ∼1:2 in the P_r forms of the noncovalent BV adduct and the covalent PCB adduct appears to be fortuitous, since the respective electronic configurations are completely different. The physical origin of the change in this ratio upon covalent attachment remains thus speculative. We note that the ratio of Q and Soret band ellipticities also differs considerably for the P_r forms of covalent PCB adducts of different phytochrome species: While Cph1 displays a ratio of ∼1:1 (*24*), the CD spectrum of the V249C mutant of Agp1 is characterized by a ratio of ∼1:2 (this work). These differences observed for adducts with identical electronic configurations could arise from different tilts of the pyrrole rings induced by the specific protein−cofactor interactions. The lack of structural data on the PCB adduct of Agp1-V249C does not allow verification of this hypothesis.

The strong increase in the ellipticity of both main absorption bands upon covalent attachment of BV and the decrease in the ellipticity of the Q-band upon covalent attachment of PCB may be due to partial rotations of the A ring in the formation of the covalent bonds in opposite directions according to the different positions of the two cysteines to which these chromophores are bound. Structural studies showed that these cysteines are on opposite sides of coplanar rings B and C (*29*). However, the crystal structures of *Dr*BphP (*30*) and Cph1 (*34*) do not display large differences in the tilt angle of the A ring of the covalently attached BV and PCB chromophores (∼15° vs 10°), arguing against the ring A rotation as the origin of substantial changes in the ellipticities upon covalent binding. On the other hand, the rearrangement of the double bond from C2=C3 to C3=$C3^1$ upon covalent attachment of BV as suggested from the high-resolution structure of the CBD of *Dr*BphP (*30*) occurs in the plane of ring A and may thus not lead to a largely increased ellipticity. Control measurements with a noncovalent BV adduct of Agp1-WT in which Cys20 is chemically blocked by thiol reactive agents led to CD spectra almost identical to those of Agp1-C20A, excluding steric effects from the substitution of cysteine with alanine in the noncovalent BV adduct of the mutant. The loss of the C3=$C3^1$ bond upon covalent attachment of PCB is associated with a reduced contribution of the tilted A ring to the overall CD signal, making a decrease in ellipticity more plausible than the opposite effect with BV. Apart from the shorter π-conjugation system that only partially includes the A ring, the smaller ellipticities of the covalent PCB adducts (Cph1 and Agp1-V249C) with respect to that of the covalent BV adduct of Agp1-WT could arise from a smaller out-of-plane rotation of ring D as suggested from the crystal structures of Cph1 and the two bacteriophytochromes *Dr*BphP and *Rp*BphP3 (26° vs 40−50°). However, the smaller tilt angle of the D ring of PCB in Cph1 was attributed to interactions with residues of the PHY domain (*34*), implying that the larger tilt of the D ring of BV in the bacteriophytochromes is an artifact from the missing PHY domain in these structures.

Among the CD spectra of the P_{fr} forms of the four adducts of Agp1 investigated in this study, only that of the covalent PCB adduct shows sign reversal of the Q-band ellipticity with respect to the P_r form. In the three other adducts, sign reversal upon photoconversion is absent, and the Q-band ellipticity in the P_{fr} state is close to zero. The CD spectrum of the P_{fr} form of the covalent Agp1−PCB adduct closely resembles that of the covalent Cph1−PCB adduct (see ref (*24*)). Sign reversal has also been observed in the CD spectra of plant phytochrome (*38*, *39*), although the relative amplitude of the positive Q-band ellipticity in the P_{fr} state is considerably lower than that of the covalent PCB adducts of Agp1 and Cph1. In all of these cases, the Q-band maxima of the absorption and CD spectra are approximately at the same wavelength.

In the noncovalent PCB adduct of Cph1, the formation of the P_{fr}-like photoproduct was also associated with sign reversal in ellipticity, but the positive CD band of the photoproduct was blue-shifted with respect to the negative CD band in the P_r state (*24*). This positive CD band was tentatively assigned to a surface-bound PCB species centered near 580 nm and a contribution from P_{fr} with a maximum near 650 nm. Because of the mismatch with the absorption spectrum (λ_{max} ∼ 730 nm), the latter assignment was probably incorrect and the observed positive CD band arose entirely from the surface-bound PCB species. Therefore, we conclude that the sign reversal of the Q-band CD upon photoconversion is restricted to covalent PCB and PϕB adducts, providing a distinctive feature compared to the respective noncovalent adducts. In the former adducts, the contribution of the A ring to the CD signal is small due to the truncated π-conjugation system that extends merely to the C4=C5 bond (see above). The observed sign reversal is thus predominantly due to the *Z*−*E* isomerization of the C−D methine bridge that occurs in the primary photochemical event. This conclusion is consistent with similar observations in the photochromic phycobiliprotein α-phycoerythrocyanin (*47*) in which the structures of the *Z* and *E* forms mainly differ by a large out-of-plane rotation of ring D of the phycoviolobilin chromophore (*48*).

Sign reversal was also observed with the 5*Zs* locked BV adduct of Agp1 in which the A ring of the chromophore was immobilized to an approximately coplanar geometry of the A−B methine bridge (*37*). The photoproduct of this adduct was blue-shifted and was assigned to a Meta-R_A-like state. There it was argued that the lock at the A−B methine bridge prevents the thermal rotation from *syn* to *anti* that proceeds in the subsequent Meta-R_A to Meta-R_C transition of the unlocked BV adduct and leads to a compensation of the Q-band CD. Modeling studies with the

coordinates of the closely related *Dr*BphP showed that this rotation is in principle possible and not restricted by the protein (*32*). However, recent NMR (*35*) and crystallographic (*36*) studies on covalent PCB and BV adducts, respectively, provided evidence that the 5*Zs* configuration/conformation is preserved in the P_{fr} form. Magic-angle spinning NMR investigations showed that no major effect occurs around C5 in the A−B methine bridge, reflecting a loss of conformational freedom along rings A and B (*49*). Moreover, the crystal structures of the P_r form of Cph1 and the bacteriophytochromes indicate close packing around chromophore rings A−C, ruling out major conformational changes in that region of the chromophore without associated dramatic changes in the protein (*34*). On the other hand, NMR studies revealed a surprisingly high mobility of the chromophore in the P_r state, allowing substantial rotations of the pyrrole rings (*50*−*52*). FTIR studies on plant phytochrome suggested an environmental change in the ring A carbonyl group and/or a twist of the A−B methine bridge (*53*).

If all the arguments are combined, the most likely scenario is that in which only a partial rotation of the A ring occurs in the thermal relaxation pathway during the P_r to P_{fr} photoconversion. This would explain the inhibition of P_{fr} formation in the locked 5*Zs* adduct of Agp1 (*32*, *37*) and the absence of sign reversal of the Q-band CD in adducts in which the A ring contributes substantially by double bonds between C2 and C3 (noncovalent BV adduct) or between C3 and $C3^1$ (covalent BV and noncovalent PCB adduct) to the CD spectrum. It is currently unknown how large the partial rotation of ring A needs to be to compensate for the reversal of the Q-band CD from isomerization of the C−D methine bridge. In the covalent PCB and PϕB adducts, the CD spectrum is virtually insensitive to rotations of ring A due to its minor contribution to the π-conjugation system. We note that the spectral changes during P_r to P_{fr} photoconversion are very similar in the covalent and noncovalent adducts of Agp1 (see the results from flash spectroscopy). It is thus reasonable to assume that a common mechanism of photoactivation exists, including the same changes in the geometry of the chromophore. These results from CD spectroscopy and their interpretation are consistent with this notion.

An alternative explanation for the absence of sign reversal of the Q-band CD in BV binding phytochromes was proposed, after submission of this paper, on the basis of CD spectroscopy and ab initio calculations (*54*). In this study, different orientations ("facial dispositions") of the D ring plane in the respective P_{fr} states of BV and phytobilin (PCB and PϕB) binding phytochromes were proposed to be responsible for the difference in sign of the Q-band CD. However, in our study, the absence of sign reversal of the Q-band CD was also demonstrated for the noncovalent PCB adduct of Agp1. Moreover, we showed that the amplitude spectra and kinetics are very similar in the covalent and noncovalent PCB adducts of Agp1. Therefore, different orientations of the D ring plane in the respective P_{fr} states and different directions of bilin D ring rotation upon photoisomerization as required in the model of ref (*54*) are quite unlikely.

Relaxation Processes in the P_r to P_{fr} Photoconversion. The P_r to P_{fr} photoconversion in the covalent and noncovalent bilin adducts of Agp1 phytochrome was investigated by time-resolved absorption spectroscopy. For the noncovalent BV adduct (Agp1-C20A), three relaxation components, kinetically and spectrally very similar to those of the covalent BV adduct (Agp1-WT), were observed. It is thus reasonable to assign these components to the same transitions as in the covalent BV adduct involving Lumi-R, Meta-R_A, and Meta-R_C intermediates. The good agreement of the extrapolated initial difference spectra, ΔA_{init}, of the covalent and noncovalent adducts indicates that the primary photochemical event is unaffected by the covalent attachment at ring A of the chromophore and probably does not involve structural changes in this part of the chromophore. This is consistent with the generally accepted mechanism of the localized *Z*−*E* photoisomerization of the C−D methine bridge (*16*, *17*, *28*, *55*, *56*). However, recent results from ultrafast vibrational spectroscopy of Cph1 suggest that in addition changes in the A−B methine bridge (low bond order torsional angle changes of the C5−C6 bond) occur in the formation of the Lumi-R intermediate (*57*). Significant differences between covalent and noncovalent BV adducts occur in the amplitudes of the Meta-R_A to Meta-R_C transition that is accelerated, moreover, by a factor of ~3 in the noncovalent adduct. These spectral and kinetic differences may indicate that the Meta-R_A to Meta-R_C transition is associated with structural changes near ring A of the chromophore such as a partial rotation of ring A as proposed on the basis of CD spectra of covalent and noncovalent adducts of Agp1 (see above). We conclude that in the absence of the covalent attachment, the structural changes are facilitated. Proton release and uptake remain kinetically correlated with the formation and decay of Meta-R_C in the absence of the covalent attachment. Proton reuptake in the noncovalent adduct was also associated with a reduced amplitude, implying net acidification in the P_r to P_{fr} photoconversion. The main difference between the covalent and noncovalent BV adducts of Agp1 is the much lower photostability of the noncovalent adduct. The formation of the irreversibly bleached photoproduct most likely proceeds as a branching reaction from the electronically excited state. The photochemical mechanism of protection in the covalent BV adduct remains an unexplained issue, though.

For the covalent and noncovalent PCB adducts, four relaxation components were obtained from a global analysis of data at multiple wavelengths. The fourth component reflects an only minor contribution to the formation of P_{fr}. The three other components and the extrapolated initial difference spectra show the same spectral characteristic that was obtained for the BV adducts. Apart from an ~15 nm blue shift due to the shorter π-conjugation system, the amplitude spectra of the noncovalent PCB adduct are almost congruent to those of the covalent BV adduct. The amplitude spectra of the covalent PCB adduct exhibit apparent deviations from those of the noncovalent PCB adduct in the second and third components (B_2 and B_3, respectively). These deviations are probably due to the near degeneracy of the related time constants (720 μs and 1.9 ms) leading to partial exchange of the amplitudes. We note that the sums of B_2 and B_3 are again very similar in both PCB adducts (see Figure S7 of the Supporting Information), including the major contributions to the formation of the respective P_{fr} states.

The formation of P_{fr} in the PCB adducts is faster by 2 orders of magnitude with respect to the BV adducts of Agp1. The fact that adducts with the non-natural PCB undergo faster kinetics than those with natural BV suggests that evolutionary pressure favors slower kinetics, although faster transitions are principally possible. Since the acceleration occurs similarly in the covalent and noncovalent PCB adducts, it is not due to the binding mode of the bilin chromophore as proposed for the noncovalent PCB adduct of CphB from the cyanobacterium *Calothrix* (*25*). The absence of the 18-vinyl group is apparently responsible for this kinetic effect. A considerable acceleration of the Meta-R_C to P_{fr} transition was

also observed with the covalent 18Et-BV adduct of Agp1 in which the 18-vinyl group is replaced with an ethyl group as in PCB (*37*). These observations suggest that the Meta-R_C state in the BV adduct of Agp1 is stabilized by an interaction of the protein moiety with the $C18^1$=$C18^2$ bond, implying a conformational change in ring D in the respective transition. The kinetic effect of the 18-vinyl group, also known from the respective adducts of plant phytochrome (*58*) and Cph1 (*19*), will be investigated in more detail in future work. Interestingly, the formation of P_{fr} in the covalent PCB adduct of Cph1 proceeds in the same time range as in the covalent BV adduct of Agp1 and is thus considerably slower than in the covalent PCB adduct of Agp1. This discrepancy between PCB adducts of different phytochrome species shows that the final step in the P_r to P_{fr} photoconversion is regulated by further protein−chromophore interactions. The covalent PCB adducts of Cph1 and Agp1 differ furthermore in the amplitude spectra for the first two significant relaxation components in the P_r to P_{fr} photoconversion. In the Cph1−PCB adduct, the first component with a time constant of ~300 μs is associated with a red shift and the second component with a time constant of ~3 ms shows mainly an absorption decrease in the Q-band (*19*, *20*). This apparent reversal in the sequence of the first two transitions indicates that the P_r to P_{fr} photoconversion in Cph1 proceeds via an exceptional pathway while phytochromes phyA from plants and Agp1 from *A. tumefaciens* share a common relaxation pathway. We note in this context that, according to phylogenetic analyses, plant phytochromes have not evolved from cyanobacterial predecessors but rather from other bacterial phytochromes and that the switch of the chromophore binding site has apparently taken place independently in plants and cyanobacteria (*11*). It appears as if the specific chromophore−protein interactions play a more dominant role than the type of bilin chromophore (BV, PCB, or PϕB) or the mode of noncovalent and covalent attachment (vinyl or ethylidene group involved).

The dye signal, detected in an unbuffered solution of the covalent PCB adduct of Agp1, displays only an apparent proton release phase. However, simultaneous fits showed that the dye signal is a superposition of a rise and a decay component with time constants of 1.1 and 2.7 ms, respectively. These results suggest that proton release and uptake also occur in the covalent PCB adduct of Agp1 and are also associated with the rise and decay of the Meta-R_C intermediate. The stoichiometry of net proton release of 0.9 ± 0.2 does not allow us to distinguish between fractional and integer stoichiometry. Substoichiometric proton release would be consistent with the proposed mechanism of stoichiometric proton release and subsequent partial reuptake as observed with the covalent BV adduct of Agp1 and the covalent PCB adduct of Cph1. Within experimental error, stoichiometric net proton release, i.e., one proton per photoconverted molecule, cannot be excluded, however. Since proton release and uptake are coupled to transient deprotonation and reprotonation of the BV chromophore in Agp1 (*21*), it is reasonable to assume that the photoconversion of the PCB adduct also involves these proton translocation steps.

Role of the N-Terminal Amino Acids in Agp1. The BV adduct of the M15Δ18N mutant of Agp1 showed striking similarities to that of the C20A mutant in the absorption and CD spectra, transient absorption changes, protonation kinetics, and photobleaching pattern. These strong similarities suggest that they arise from the absence of the covalent linkage of the BV chromophore as unambiguously proven only for the C20A mutant so far (*4*). However, analysis of the M15Δ18N mutant by sodium dodecyl sulfate−polyacrylamide gel electrophoresis (SDS−PAGE) and Zn^{2+}-induced fluorescence, which is commonly used as evidence of covalent associations of bilin chromophores (*59*, *60*), indicated a covalently bound chromophore (data not shown). SDS desalting column separation with M15Δ18N then revealed that at least the major fraction of the BV chromophore is noncovalently attached, confirming the preliminary conclusion from the spectroscopic and kinetic data. This result implies that Zn^{2+} fluorescence on SDS−PAGE initially led to false conclusions: on these gels, a fluorescent band was observed at the position of the protein (data not shown). This fluorescence could have been due to a noncovalent binding of the chromophore to the protein in the stacking gel. A further common property of the M15Δ18N and C20A mutants is the rather rapid P_{fr} to P_r dark reversion that has already been described for M15Δ18N (*40*) and has been observed with the C20A mutant as well (data not shown).

Recently, an analogous mutant of the closely related *Dr*BphP was described that lacks the first 20 N-terminal amino acids, keeping three amino acids upstream of cysteine 24, the binding site of this phytochrome (*61*). On the basis of zinc-induced fluorescence following SDS−PAGE, these authors concluded that BV binds covalently in this mutant. However, the results from this assay could also have been misleading. In fact, the spectra of the deletion mutant of *Dr*BphP upon red light illumination suggest properties similar to those of the M15Δ18N mutant of Agp1, including the lower absorption of the Q-band of the P_{fr} form, as well as the apparent bleach of the Q-band of the P_r form and the formation of blue-shifted irreversible photoproducts due to photobleaching from oversaturating illumination. Therefore, we propose that the BV chromophore in the ΔN1−20 deletion mutant of *Dr*BphP is also noncovalently attached.

We note that the inability to form a covalent attachment in Agp1 phytochrome is obviously due to amino acids 11−19, since deletion of amino acids 2−10 does not prevent covalent binding of the BV chromophore (*12*). Two alternative explanations could account for this observation. (i) Amino acids 11−19 play an important role in the autolyase activity of this bacterial phytochrome, or (ii) the deletion of these amino acids leads to a rearrangement of cysteine 20 such that the vinyl group at ring A of the noncovalently bound BV is no longer in the proximity of the SH group.

Role of Covalent Attachment of the Bilin Chromophore. Although we and others showed that covalent attachment of the chromophore is not required for the functional integrity of phytochromes, there are remarkable differences between noncovalent and covalent adducts. In Agp1, covalent attachment of BV is associated with an increase in the extinction coefficient, results in a bathochromic shift of the P_{fr} maximum (*4*), and affects photoconversion kinetics significantly. In Cph1, the noncovalent adduct differs considerably from the covalent one by an ~30 nm red shift in the Q-band absorption (*24*). It was recently found that the covalent binding is also important for the dark conversion of the bathyphytochrome Agp2 (*62*). At low intracellular concentrations, the covalent attachment prevents dissociation of the chromophore−protein complex. One obvious function of the covalent attachment in native phytochrome is to protect the receptor protein from irreversible photobleaching: the chromophore in noncovalent BV adducts was specifically sensitive to photodegradation. However, the noncovalent PCB adduct

of Agp1 was quite photostable, although BV is the natural chromophore of Agp1. We note in this context that those organisms that perform oxygenic photosynthesis, i.e., plants and cyanobacteria, use either PϕB or PCB as a phytochrome chromophore. These organisms are most susceptible to photodamage events because they typically grow in bright sunlight and produce oxygen which will increase phototoxic effects. Tetrapyrroles such as heme (*63*), chlorophylls (*64*), or biosynthesis intermediates (*65*) are often the cause or target of photodamage. Biliverdin adducts might in general be more sensitive to photodamage than PCB adducts, and the replacement of the chromophore during evolution might have resulted in a prolonged lifetime of phytochrome in cyanobacteria and plants.

ACKNOWLEDGMENT

We thank Harald Otto (Physics Department, Freie Universität Berlin) for helpful discussions and Steffi Noack and Norbert Michael (Biology Department, Freie Universität Berlin) for preparative assistance.

SUPPORTING INFORMATION AVAILABLE

Seven figures. This material is available free of charge via the Internet at http://pubs.acs.org.

REFERENCES

1. Kendrick, R. E., and Kronenberg, G. H. M., Eds. (1994) Photomorphogenesis in Plants, 2nd ed., Kluwer Academic Publishers, Dordrecht, The Netherlands.
2. Vierstra, R., and Karniol, B. (2005) Phytochromes in Microorganisms. In Handbook of Photosensory Receptors (Briggs, W. R., and Spudich, J. L., Eds.) pp 171−195, Wiley Verlag, Weinheim, Germany.
3. Bhoo, S. H., Davis, S. J., Walker, J., Karniol, B., and Vierstra, R. D. (2001) Bacteriophytochromes are photochromic histidine kinases using a biliverdin chromophore. *Nature 414*, 776–779.
4. Lamparter, T., Michael, N., Mittmann, F., and Esteban, B. (2002) Phytochrome from *Agrobacterium tumefaciens* has unusual spectral properties and reveals an N-terminal chromophore attachment site. *Proc. Natl. Acad. Sci. U.S.A. 99*, 11628–11633.
5. Quest, B., Hübschmann, T., Sharda, S., Tandeau de Marsac, N., and Gärtner, W. (2007) Homologous expression of a bacterial phytochrome. The cyanobacterium *Fremyella diplosiphon* incorporates biliverdin as a genuine, functional chromophore. *FEBS J. 274*, 2088–2098.
6. Froehlich, A. C., Noh, B., Vierstra, R. D., Loros, J., and Dunlap, J. C. (2005) Genetic and molecular analysis of phytochromes from the filamentous fungus *Neurospora crassa*. *Eukaryotic Cell 4*, 2140–2152.
7. Brandt, S., von Stetten, D., Günther, M., Hildebrandt, P., and Frankenberg-Dinkel, N. (2008) The Fungal Phytochrome FphA from *Aspergillus nidulans*. *J. Biol. Chem. 283*, 34605–34614.
8. Hübschmann, T., Börner, T., Hartmann, E., and Lamparter, T. (2001) Characterisation of the Cph1 holo-phytochrome from *Synechocystis* sp. PCC 6803. *Eur. J. Biochem. 268*, 2055–2063.
9. Wu, S. H., McDowell, M. T., and Lagarias, J. C. (1997) Phycocyanobilin is the natural precursor of the phytochrome chromophore in the green alga *Mesotaenium caldariorum*. *J. Biol. Chem. 272*, 25700–25705.
10. Rüdiger, W., and Thümmler, F. (1994) The phytochrome chromophore. In Photomorphogenesis in Plants (Kendrick, R. E., and Kronenberg, G. H. M., Eds.) 2nd ed., pp 51−69, Kluwer Academic Publishers, Dordrecht, The Netherlands.
11. Lamparter, T. (2004) Evolution of cyanobacterial and plant phytochromes. *FEBS Lett. 573*, 1–5.
12. Lamparter, T., Carrascal, M., Michael, N., Martinez, E., Rottwinkel, G., and Abian, J. (2004) The BV chromophore binds covalently to a conserved cysteine residue in the N-terminus of *Agrobacterium* phytochrome Agp1. *Biochemistry 43*, 3659–3669.
13. Lamparter, T., Michael, N., Caspani, O., Miyata, T., Shirai, K., and Inomata, K. (2003) Biliverdin binds covalently to *Agrobacterium* phytochrome Agp1 via its ring A vinyl side chain. *J. Biol. Chem. 278*, 33786–33792.
14. Thümmler, F., and Rüdiger, W. (1983) Models for the photoreversibility of phytochrome Z,E isomerization of chromopeptides from phycocyanin and phytochrome. *Tetrahedron 39*, 1943–1951.
15. Farrens, D. L., Holt, R. E., Rospendowski, B. N., Song, P.-S., and Cotton, T. M. (1989) Surface-enhanced resonance Raman scattering spectroscopy applied to phytochrome and its model compounds. 2. Phytochrome and phycocyanin chromophores. *J. Am. Chem. Soc. 111*, 9162–9169.
16. Matysik, J., Hildebrandt, P., Schlamann, W., Braslavsky, S. E., and Schaffner, K. (1995) Fourier-transform resonance Raman spectroscopy of intermediates of the phytochrome photocycle. *Biochemistry 34*, 10497–10507.
17. Andel, F.III, Lagarias, J. C., and Mathies, R. A. (1996) Resonance Raman analysis of chromophore structure in the Lumi-R photoproduct of phytochrome. *Biochemistry 35*, 15997–16008.
18. Zhang, C.-F., Farrens, D. L., Björling, S. C., Song, P.-S., and Kliger, D. S. (1992) Time-resolved absorption studies of native etiolated oat phytochrome. *J. Am. Chem. Soc. 114*, 4569–4580.
19. Remberg, A., Lindner, I., Lamparter, T., Hughes, J., Kneip, K., Hildebrandt, P., Braslavsky, S. E., Gärtner, W., and Schaffner, K. (1997) Raman spectroscopic and light-induced kinetic characterization of a recombinant phytochrome of the cyanobacterium *Synechocystis*. *Biochemistry 36*, 13389–13395.
20. van Thor, J. J., Borucki, B., Crielaard, W., Otto, H., Lamparter, T., Hughes, J., Hellingwerf, K. J., and Heyn, M. P. (2001) Light-induced proton release and proton uptake reactions in the cyanobacterial phytochrome Cph1. *Biochemistry 40*, 11460–11471.
21. Borucki, B., von Stetten, D., Seibeck, S., Lamparter, T., Michael, N., Mroginski, M. A., Otto, H., Murgida, D. H., Heyn, M. P., and Hildebrandt, P. (2005) Light-induced proton release of phytochrome is coupled to the transient deprotonation of the tetrapyrrole chromophore. *J. Biol. Chem. 280*, 34358–34364.
22. Eilfeld, P., and Rüdiger, W. (1985) Absorption spectra of phytochrome intermediates. *Z. Naturforsch. 40c*, 109–114.
23. Foerstendorf, H., Mummert, E., Schäfer, E., Scheer, H., and Siebert, F. (1996) Fourier-transform infrared spectroscopy of phytochrome: Difference spectra of the intermediates of the photoreactions. *Biochemistry 35*, 10793–10799.
24. Borucki, B., Otto, H., Rottwinkel, G., Hughes, J., Heyn, M. P., and Lamparter, T. (2003) Mechanism of Cph1 phytochrome assembly from stopped-flow kinetics and circular dichroism. *Biochemistry 42*, 13684–13697.
25. Jorissen, H. J. M. M., Quest, B., Remberg, A., Coursin, T., Braslavsky, S. E., Schaffner, K., Tandeau de Marsac, N., and Gärtner, W. (2002) Two independent, light-sensing two-component systems in a filamentous cyanobacterium. *Eur. J. Biochem. 269*, 2662–2671.
26. Jorissen, H. J. M. M., Quest, B., Lindner, I., Tandeau de Marsac, N., and Gärtner, W. (2002) Phytochromes with noncovalently bound chromophores: The ability of apophytochromes to direct tetrapyrrole photoisomerization. *Photochem. Photobiol. 75*, 554–559.
27. Lamparter, T., and Michael, N. (2005) *Agrobacterium* phytochrome as an enzyme for the production of *ZZE* bilins. *Biochemistry 44*, 8461–8469.
28. Inomata, K., Hammam, M. A. S., Kinoshita, H., Murata, Y., Khawn, H., Noack, S., Michael, N., and Lamparter, T. (2005) Sterically locked synthetic bilin derivatives and phytochrome Agp1 from *Agrobacterium tumefaciens* form photoinsensitive Pr- and Pfr-like adducts. *J. Biol. Chem. 280*, 24491–24497.
29. Wagner, J. R., Brunzelle, J. S., Forest, K. T., and Vierstra, R. D. (2005) A light-sensing knot revealed by the structure of the chromophore-binding domain of phytochrome. *Nature 438*, 325–331.
30. Wagner, J. R., Zhang, J., Brunzelle, J. S., Vierstra, R. D., and Forest, K. T. (2007) High resolution structure of *Deinococcus* bacteriophytochrome yields new insights into phytochrome architecture and evolution. *J. Biol. Chem. 282*, 12298–12309.
31. Yang, X., Stojkovic, E. A., Kuk, J., and Moffat, K. (2007) Crystal structure of the chromophore binding domain of an unusual bacteriophytochrome, RpBphP3, reveals residues that modulate photo conversion. *Proc. Natl. Acad. Sci. U.S.A. 104*, 12571–12576.
32. Inomata, K., Noack, S., Hammam, M. A. S., Khawn, H., Kinoshita, H., Murata, Y., Michael, N., Scheerer, P., Krauss, N., and Lamparter, T. (2006) Assembly of synthetic locked chromophores with *Agrobacterium* phytochromes Agp1 and Agp2. *J. Biol. Chem. 281*, 28162–28173.
33. von Stetten, D., Seibeck, S., Michael, N., Scheerer, P., Mroginski, M. A., Murgida, D. H., Krauss, N., Heyn, M. P., Hildebrandt, P., Borucki, B., and Lamparter, T. (2007) Highly conserved residues D197 and H250 in Agp1 phytochrome control the proton affinity of the chromophore and Pfr formation. *J. Biol. Chem. 282*, 2116–2123.

34. Essen, L.-O., Mailliet, J., and Hughes, J. (2008) The structure of a complete phytochrome sensory module in the Pr ground state. *Proc. Natl. Acad. Sci. U.S.A. 105*, 14709–14714.
35. Hahn, J., Strauss, H. M., and Schmieder, P. (2008) Heteronuclear NMR investigation on the structure and dynamics of the chromophore binding pocket of the cyanobacterial phytochrome Cph1. *J. Am. Chem. Soc. 130*, 11170–11178.
36. Yang, X., Kuk, J., and Moffat, K. (2008) Crystal structure of *Pseudomonas aeruginosa* bacteriophytochrome: Photoconversion and signal transduction. *Proc. Natl. Acad. Sci. U.S.A. 105*, 14715–14720.
37. Seibeck, S., Borucki, B., Otto, H., Inomata, K., Khawn, H., Kinoshita, H., Michael, N., Lamparter, T., and Heyn, M. P. (2007) Locked 5*Z*s-biliverdin blocks the Meta-R_A to Meta-R_C transition in the functional cycle of bacteriophytochrome Agp1. *FEBS Lett. 581*, 5425–5429.
38. Song, P.-S., Chae, Q., and Gardner, J. D. (1979) Spectroscopic properties and chromophore conformations of the photomorphogenic receptor: Phytochrome. *Biochim. Biophys. Acta 576*, 479–495.
39. Litts, J. C., Kelly, J. M., and Lagarias, J. C. (1983) Structure-function studies on phytochrome. *J. Biol. Chem. 258*, 11025–11031.
40. Noack, S., Michael, N., Rosen, R., and Lamparter, T. (2007) Protein conformational changes of *Agrobacterium* phytochrome Agp1 during chromophore assembly and photoconversion. *Biochemistry 46*, 4164–4176.
41. Scheerer, P., Michael, N., Park, J. H., Noack, S., Förster, C., Hammam, M. A. S., Inomata, K., Choe, H. W., Lamparter, T., and Krauss, N. (2006) Crystallization and preliminary X-ray crystallographic analysis of the N-terminal photosensory module of phytochrome Agp1, a BV-binding photoreceptor from *Agrobacterium tumefaciens*. *J. Struct. Biol. 153*, 97–102.
42. Borucki, B., Otto, H., Meyer, T. E., Cusanovich, M. A., and Heyn, M. P. (2005) Sensitive circular dichroism marker for the chromophore environment of photoactive yellow protein: Assignment of the 307 and 318 nm bands to the $n \rightarrow \pi^*$ transition of the carbonyl. *J. Phys. Chem. B 109*, 629–633.
43. Borucki, B., Devanathan, S., Otto, H., Cusanovich, M. A., Tollin, G., and Heyn, M. P. (2002) Kinetics of proton uptake and dye binding by photoactive yellow protein in wildtype and in the E46Q and E46A mutants. *Biochemistry 41*, 10026–10037.
44. Borucki, B. (2006) Proton transfer in the photoreceptors phytochrome and photoactive yellow protein. *Photochem. Photobiol. Sci. 5*, 553–566.
45. Rockwell, N. C., Njuguna, S. L., Roberts, L., Castillo, E., Parson, V. L., Dwojak, S., Lagarias, J. C., and Spiller, S. C. (2008) A second conserved GAF domain cysteine is required for the blue/green photoreversibility of cyanobacteriochrome Tlr0924 from *Thermosynechococcus elongatus*. *Biochemistry 47*, 7304–7316.
46. Murgida, D. H., von Stetten, D., Hildebrandt, P., Schwinté, P., Siebert, F., Sharda, S., Gärtner, W., and Mroginski, M. A. (2007) The chromophore structures of the Pr States in plant and bacterial phytochromes. *Biophys. J. 93*, 2410–2417.
47. Zhao, K.-H., and Scheer, H. (1995) Type I and type II reversible photochemistry of phycoerythrocyanin α-subunit from *Mastigocladus laminosus* both involve *Z*,*E* isomerisation of phycoviolobilin chromophore and are controlled by sulfhydryls in apoprotein. *Biochim. Biophys. Acta 1228*, 244–253.
48. Schmidt, M., Patel, A., Zhao, Y., and Reuter, W. (2007) Structural basis for the photochemistry of α-phycoerythrocyanin. *Biochemistry 46*, 416–423.
49. Rohmer, T., Lang, C., Hughes, J., Essen, L.-O., Gärtner, W., and Matysik, J. (2008) Light-induced chromophore activity and signal transduction in phytochromes observed by ^{13}C and ^{15}N magic-angle spinning NMR. *Proc. Natl. Acad. Sci. U.S.A. 105*, 15229–15234.
50. Strauss, H. M., Hughes, J., and Schmieder, P. (2005) Heteronuclear solution-state NMR studies of the chromophore in cyanobacterial phytochrome Cph1. *Biochemistry 44*, 8244–8250.
51. Rohmer, T., Strauss, H., Hughes, J., de Groot, H., Gärtner, W., Schmieder, P., and Matysik, J. (2006) ^{15}N MAS NMR studies of Cph1 phytochrome: Chromophore dynamics and intramolecular signal transduction. *J. Phys. Chem. B 110*, 20580–20585.
52. Cornilescu, G., Ulijasz, A. T., Cornilescu, C. C., Markley, J. L., and Vierstra, R. D. (2008) Solution structure of a cyanobacterial phytochrome GAF domain in the red-light-absorbing ground state. *J. Mol. Biol. 383*, 403–413.
53. Foerstendorf, H., Benda, C., Gärtner, W., Storf, M., Scheer, H., and Siebert, F. (2001) FTIR studies of phytochrome photoreactions reveal the C=O bands of the chromophore: Consequences for its protonation states, conformation, and protein interaction. *Biochemistry 40*, 14952–14959.
54. Rockwell, N. C., Shang, L., Martin, S. S., and Lagarias, J. C. (2009) Distinct classes of red/far-red photochemistry within the phytochrome superfamily. *Proc. Natl. Acad. Sci. U.S.A. 106*, 6123–6127.
55. Rüdiger, W., Thümmler, F., Cmiel, E., and Schneider, S. (1983) Chromophore structure of the physiologically active form (P_{fr}) of phytochrome. *Proc. Natl. Acad. Sci. U.S.A. 80*, 6244–6248.
56. Schumann, C., Gross, R., Michael, N., Lamparter, T., and Diller, R. (2007) Sub-picosecond mid-infrared spectroscopy of phytochrome Agp1 from *Agrobacterium tumefaciens*. *ChemPhysChem. 8*, 1657–1663.
57. van Thor, J. J., Ronayne, K. L., and Towrie, M. (2007) Formation of the early photoproduct Lumi-R of cyanobacterial phytochrome Cph1 observed by ultrafast mid-infrared spectroscopy. *J. Am. Chem. Soc. 129*, 126–132.
58. Schmidt, P., Westphal, U. H., Worm, K., Braslavsky, S. E., Gärtner, W., and Schaffner, K. (1996) Chromophore-protein interaction controls the complexity of the phytochrome photocyle. *J. Photochem. Photobiol., B 34*, 73–77.
59. Berkelman, T. R., and Lagarias, J. C. (1986) Visualization of bilin-linked peptides and proteins in polyacrylamide gels. *Anal. Biochem. 156*, 194–201.
60. Karniol, B., Wagner, J. R., Walker, J. M., and Vierstra, R. D. (2005) Phylogenetic analysis of the phytochrome superfamily reveals distinct microbial subfamilies of photoreceptors. *Biochem. J. 392*, 103–116.
61. Wagner, J. R., Zhang, J., von Stetten, D., Günther, M., Murgida, D. H., Mroginski, M. A., Walker, J. M., Forest, K. T., Hildebrandt, P., and Vierstra, R. D. (2008) Mutational analysis of *Deinococcus radiodurans* bacteriophytochrome reveals key amino acids necessary for the photochromicity and proton exchange cycle of phytochromes. *J. Biol. Chem. 283*, 12212–12226.
62. Inomata, K., Khawn, H., Chen, L. Y., Kinoshita, H., Zienicke, B., Molina, I., and Lamparter, T. (2009) Assembly of *Agrobacterium* phytochromes Agp1 and Agp2 with doubly locked bilin chromophores. *Biochemistry 48*, 2817–2827.
63. Sassa, S. (2004) Why heme needs to be degraded to iron, biliverdin IX α, and carbon monoxide?. *Antioxid. Redox Signaling 6*, 819–824.
64. Mohanty, P., Allakhverdiev, S. I., and Murata, N. (2007) Application of low temperatures during photoinhibition allows characterization of individual steps in photodamage and the repair of photosystem II. *Photosynth. Res. 94*, 217–224.
65. Jung, S., Lee, H. J., Lee, Y., Kang, K., Kim, Y. S., Grimm, B., and Back, K. (2008) Toxic tetrapyrrole accumulation in protoporphyrinogen IX oxidase-overexpressing transgenic rice plants. *Plant Mol. Biol. 67*, 535–546.